ACS APPLIED MATERIALS & INTERFACES

Research Article

www.acsami.org

High-Mobility ZnO Nanorod Field-Effect Transistors by Self-Alignment and Electrolyte-Gating

Stefan Thiemann, Mathias Gruber, Irina Lokteva, Johannes Hirschmann, Marcus Halik, and Jana Zaumseil*

Institute of Polymer Materials, Friedrich-Alexander Universität Erlangen-Nürnberg, Martensstraße 7, D-91058 Erlangen, Germany

Supporting Information

ABSTRACT: High mobility, solution-processed field-effect transistors are important building blocks for flexible electronics. Here we demonstrate the alignment of semiconducting, colloidal ZnO nanorods by a simple solvent evaporation technique and achieve high electron mobilities in field-effect transistors at low operating voltages by electrolyte-gating with ionic liquids. The degree of alignment varies with nanorod length, concentration and solvent evaporation rate. We find a strong dependence of electron mobility on the degree of alignment but less on the length of the nanorods. Maximum field-effect mobilities reach up to 9 $cm^2 V^{-1} s^{-1}$ for optimal alignment. Because of the low process temperature (150 °C), ZnO nanorod thin films are suitable for application on flexible polymer substrates.

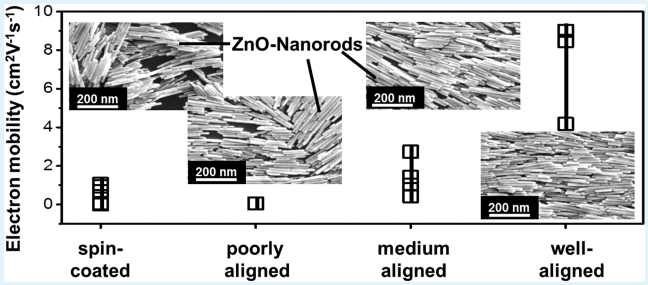

KEYWORDS: *field-effect transistors, zinc oxide, nanorods, alignment, electrolyte gating, ionic liquid*

INTRODUCTION

Producing high-performance thin-film transistors at low temperatures, over large areas, and in a cost-efficient way is one of the major challenges for flexible electronics. Several approaches with regard to the semiconducting layer have been pursued: organic semiconductors, which show moderate mobilities;[1] networks of semiconducting single-walled carbon nanotubes, with high mobilities but inferior on/off ratios;[2] and transparent conducting oxides (TCO), which exhibit high mobilities but are often produced at rather high temperatures.[3] A viable alternative could be colloidal dispersions of inorganic semiconductor nanoparticles, which can be used as printable, semiconducting inks and processed at low temperatures. Using improved synthesis methods they can be obtained routinely in large amounts, with high purity and high monodispersity.[4] Various colloidal semiconductors, e.g., CdSe,[5] PbS,[6] PbSe,[7,8] and ZnO[9,10] have been applied successfully in field-effect transistors (FET). However, FETs based on nanoparticles often show low carrier mobilities, depending on the degree of order within the film, type of ligands, and post-treatment.[4] Insulating ligands, which are necessary for stable colloidal dispersions, lead to large hopping barriers and thus low mobilities. This issue was only recently overcome by Kovalenko et al. who demonstrated high mobility FETs based on metal chalcogenides-capped CdSe nanoparticles.[11,12] Another way to minimize the impact of hopping barriers in order to improve charge transport is the use of colloidal nanowires and nanorods. Several types of semiconducting nanowires (e.g., PbSe) have shown high mobilities in FETs.[6,7]

Here we study the influence of length and orientation of solution processed ZnO nanorods of 80 to 500 nm length in electrolyte-gated FETs. ZnO is an n-type semiconductor with a large bandgap (E_g = 3.36 eV). It shows high electron mobilities of 2 to 85 $cm^2 V^{-1} s^{-1}$ in thin films produced by, for example, spray-pyrolysis,[13−15] sol−gel processing[16] or sputtering.[17] Even higher mobilities are possible for epitaxially grown ZnO.[18,19] All of these methods rely on high temperatures whereas FETs based on colloidal ZnO nanoparticle inks, which are deposited at low temperatures, usually result in inferior mobilities in the range of 1×10^{-3} $cm^2 V^{-1} s^{-1}$, even when postdeposition hydrothermal growth is used as shown by Sun et al.[10] They also demonstrated that using ZnO nanorods, which self-assemble in liquid-crystalline-like domains, instead of particles gives mobilities of up to 0.023 $cm^2 V^{-1} s^{-1}$. Because the electron mobility within a single nanorod is much higher (up to 40 $cm^2 V^{-1} s^{-1}$),[20] a large-scale alignment of ZnO nanorods parallel to the transport direction could greatly improve device performance and thus compete with ZnO thin film devices produced at high temperatures.

Several methods exist to orient nanorods and nanowires over large areas or simply between source-drain electrodes, such as directed solvent evaporation, Langmuir−Blodgett trough and electric field alignment.[21] In this study, ZnO nanorods from a colloidal dispersion were aligned by a slow solvent evaporation method as previously used by Engel et al. for single-walled

Received: November 12, 2012
Accepted: February 11, 2013
Published: February 11, 2013

carbon nanotubes.[22] This alignment method is based on Onsager's theory of rigid rods,[23] which describes the tendency of rods to form a nematic liquid crystalline phase in colloidal dispersions depending on volumetric content and aspect ratio of the rods. This theory assumes equilibrium between orientation and packing entropy and predicts a minimum energy state, in which all rods are aligned. Alignment is predicted to increase with the length of the nanorods and their concentration. Note that this applies only to rods with high aspect ratios (length/width >100). Small domains of order are routinely found in spin-coated or drop-cast films of many different nanorods almost independent of the material.[24−26] However, these domains do not extend to micro- or millimeter scales, and the overall orientation of a macroscopic film is still isotropic.

To create large-scale orientation by solvent evaporation, we vertically immersed a substrate in a solution containing nanorods. A meniscus forms at the liquid−solid−air interface. During evaporation of the solvent nanorods move toward the meniscus by convection, their local concentration increases and they align themselves parallel to the contact line and are deposited on the substrate surface as illustrated in Figure 1a. The equilibrium between friction ($F_{friction}$) of the now rough surface, liquid surface tension (γ_s) and capillary force (γ_l) leads to a stick-and-slip motion of the liquid. Thus stripes of ordered nanorods are formed during the evaporation process. This mechanism has been described in detail for various colloidal dispersions as the "coffee-stain effect".[27−29]

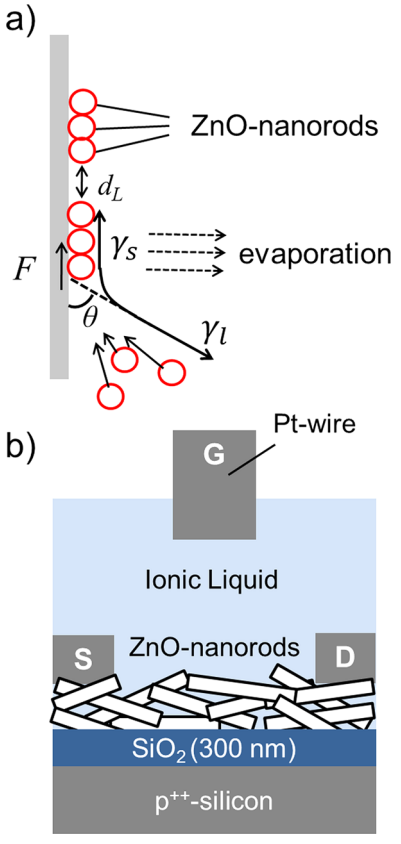

Figure 1. (a) Schematic illustration of solvent evaporation and meniscus formation for the self-assembly of ZnO nanorods at the interface. (b) Schematic illustration of ionic liquid-gated field-effect transistor with ZnO nanorods (G, gate; S, source; D, drain).

We use this effect to create large zones of self-assembled ZnO nanorods whose charge transport properties can be studied using electrolyte-gated field-effect transistors. The concept of electrolyte-gating is based on the redistribution of ions in an electrolyte when a voltage is applied to the gate electrode. This leads to the formation of electric double layers (EDL) at the surface of the gate electrode and the semiconductor. The bulk remains neutral and thus the applied gate voltage drops almost entirely over the few nm thick double layers resulting in a very high effective capacitance (several μF cm^{-2}).[30−33] Electrolyte-gating is particularly interesting for rough surfaces and nanowires. The EDL forms evenly around every surface and thus creates a uniform gating effect. Consequently electrolyte-gating is much more efficient than using a planar gate dielectric similar to wrap-around gate geometries.[20,39] Here we use the ionic liquid (IL) [EMIM]-[TFSI] (1-ethyl-3-methylimidazolium bis(trifluoromethyl-sulfonyl)imide) as the electrolyte. It has a wide electrochemical window and high ionic mobility, which allows for the accumulation of large charge carrier densities and fast switching as shown previously for various semiconductors.[30−33] We demonstrate that electrolyte-gating is an efficient way to achieve high-mobility FETs based on aligned ZnO nanorods as well as ZnO nanoparticle thin films. This allows us to compare charge transport in nanorod layers with different degrees of alignment and orientation with respect to the transport direction.

EXPERIMENTAL DETAILS

Synthesis of ZnO Nanorods. All chemicals were purchased from Sigma-Aldrich and used as received without further purification. ZnO nanorods were synthesized according to a procedure by Sun et al.[10] Briefly, 6.59 g of zinc acetate dihydrate ($ZnAc_2{\cdot}2H_2O$) and 2.70 g of potassium hydroxide (KOH) (ratio $[Zn^{2+}]/[OH^-] = 1/1.6$) were each dissolved in 60 mL of methanol at 60 °C. After mixing the two precursors the combined solution was vigorously stirred for 2 h under reflux. During this time, ZnO nanoparticles were formed and the solution turned white because of nanoparticle agglomeration. Subsequently, the dispersion was reduced to one tenth of the initial volume by bubbling dry nitrogen through it at 60 °C. The increased particle concentration initiates the growth of ZnO nanorods. During growth the dispersion was kept under reflux conditions and aliquots of the grown ZnO nanorods were taken after 1, 5, and 10 days. To hinder further growth, we added heptane/isopropanol (v/v = 5:1) in excess and samples were stored in the fridge. Prior to use, the collected ZnO nanorods were washed twice with methanol to remove byproducts and centrifuged at 7000 rpm for 30 min at 10 °C. The residue was dispersed in a chloroform−methanol mixture (v/v = 3:1) at different concentrations (0.005−0.5 wt %). The addition of the ligand butylamine (1 μL per 1 mg of ZnO) followed by sonication in a bath sonicator for 10 min or, if necessary, with a tip sonicator gave stable and homogeneous dispersions. Lengths and diameters of the nanorods after sonication were determined by transmission electron microscopy (TEM, Philips CM30) for short (24 h growth) and medium-sized (5 day growth) nanorods and by scanning electron microscopy (SEM, Zeiss Gemini Ultra 55) for the longest nanorods (10 day growth) (see Figure S1 in the Supporting Information). At least 200 individual nanorods were measured to obtain length and diameter distributions.

For the synthesis of ZnO nanoparticles, 550 mg of $ZnAc_2{\cdot}2H_2O$ and 115 mg of lithium hydroxide (LiOH) (ratio $[Zn^{2+}]/[OH^-] = 1/1.1$) were separately dissolved in 25 mL of ethanol at 80 °C and refluxed for 1 h. After cooling both solutions to 35 °C the LiOH solution was added to the zinc solution drop by drop under continuous stirring. After 2 h at 35 °C the reaction was stopped by precipitating the nanoparticles with an excess of heptane. The

dx.doi.org/10.1021/am3026739 | ACS Appl. Mater. Interfaces 2013, 5, 1656−1662

nanoparticles were collected by sedimentation and redispersed in ethanol (0.5 wt % ZnO). The average particle size was obtained by deconvolution of the absorption spectrum (see Figure S2 in the Supporting Information) using an algorithm developed by Segets et al.[34]

Device Fabrication and Characterization. All substrates (p-doped silicon wafers with 300 nm thermal SiO_2) were cleaned with H_2SO_4/H_2O_2 (v/v = 3:1), acetone, and isopropanol and hydrophilized by oxygen plasma treatment. For the controlled solvent evaporation a staining jar (height 76 mm, width 26 mm) was used, in which the substrates were positioned vertically. The prepared ZnO nanorod dispersion was carefully added and the jar was closed with a lid. Different evaporation rates were realized by putting a PTFE-spacer under the lid (higher evaporation rates) or sealing it with parafilm (slow evaporation rates). The jars were kept in a quiet place to avoid any disturbance of the liquid. After complete evaporation of the solvent, the samples were removed and annealed at 150 °C for 30 min in order to remove the butylamine ligands completely.

Spincoated films of ZnO nanorods were prepared from a 20 mg/mL dispersion in chloroform/methanol (3:1) with butylamine. They were spincoated onto Si/SiO_2 substrates at 2000 rpm for 40 s, followed by an annealing step at 150 °C in air for 30 min. ZnO nanoparticles were spincoated in a two-step process (5 s 500 rpm, 20 s 2000 rpm) and annealed at 150 °C for 30 min. Atomic force microscopy (AFM) images of the ZnO nanorod thin films were recorded with an AFM Veeco diDimension 5000 and scanning electron micrographs were taken with a Zeiss Gemini Ultra 55 SEM.

Deposition of 35 nm aluminum on top of the various ZnO layers by thermal evaporation through a polyimide shadow mask completed all devices with source and drain electrodes (perpendicular or parallel to the nanorod orientation, channel length L = 10−80 μm, channel width W = 500−4000 μm, measured W/L = 40−58). The finished devices were transferred to a dry nitrogen glovebox and annealed again at 80 °C for 30 min.

Current−voltage measurements of ZnO-FETs with SiO_2 as the dielectric (capacitance 11.5 nF cm^{-2}) and [EMIM][TFSI] as electrolyte were carried out with an Agilent 4155C semiconductor parameter analyzer at room temperature. [EMIM][TFSI] (high purity grade from Merck) was dried in vacuum (~5 × 10^{-2} mbar) at 60 °C for 12 h before storage and measurements in a nitrogen glovebox, as described elsewhere.[35] Electrolyte-gating with [EMIM][TFSI] was performed with a PDMS frame on top of the fabricated electrodes to keep the ionic liquid in place. An immersed platinum wire served as the gate electrode (see Figure 1**b**). The specific capacitance of [EMIM][TFSI] in this configuration was determined to be approximately 7 $\mu F \cdot cm^{-2}$.

RESULTS AND DISCUSSION

Alignment of ZnO Nanorods by Solvent Evaporation. Figure 2 shows the distribution of length and diameter for ZnO nanorods after short (24 h), medium (5 days), and long (10 days) growth times, which correspond to average aspect ratios of 9.5, 35.6, and 37.5, respectively, also shown in Table 1. ZnO nanorods predominantly grow along the *c*-axis of their wurtzite structure,[36] thus the length distributions shift and broaden with growth time while the diameters increase only slightly, leading to larger aspect ratios. The different aspect ratios should have an effect on the capability of alignment as well as on charge transport in thin films of ZnO nanorods.

The controlled deposition and orientation of the ZnO nanorods strongly depends on the dispersion concentration and evaporation rate, which had to be optimized. High concentrations (>0.5 wt %) led to immediate aggregation and were therefore excluded although theory would predict increased alignment. Less concentrated dispersions (0.075−0.1 wt %) experienced stick−slip motion leading to thick stripes with fanlike features, as shown in Figure S3 in the Supporting Information. However, these stripes were too thick for thin film applications and did not adhere well to the substrate. Decreasing the concentration further to 0.05 wt % resulted in parallel stripes with a film thickness of 80−200 nm. These stripes were oriented parallel to the evaporation line and individual ZnO nanorods showed similar orientation.

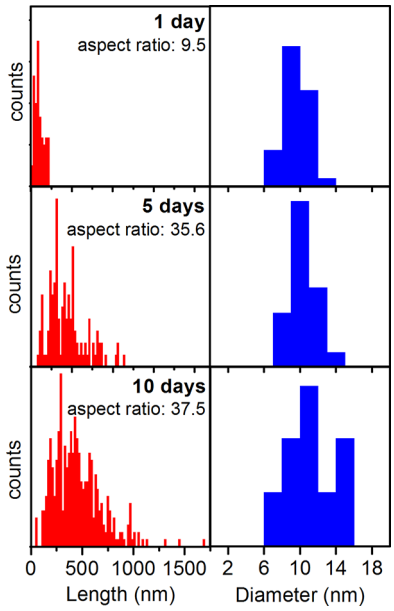

Figure 2. Length/diameter distributions and average aspect ratios of ZnO nanorods (as determined from TEM and SEM images) after (a) 24 h, (b) 5 days, and (c) 10 days of growth.

Table 1. Average Lengths, Diameters, and Aspect Ratios of ZnO Nanorods as Determined from TEM and SEM Images after 24 h, 5 Days, and 10 Days of Growth

	growth time		
	1 day	5 days	10 days
average length (nm)	87	366	480
average diameter (nm)	9.2	10.3	12.8
aspect ratio	9.5	35.6	37.5

Further, the evaporation rates had to be adjusted. We found that high evaporation rates (>4 μm/min) led to highly disordered thick stripes, whereas slow evaporation rates (<2 μm/min) resulted in thin (~100 nm) homogeneous stripes (also see Figure S3 in the Supporting Information). Therefore nanorod concentrations of 0.05 wt % and evaporation rates of less than 2 μm/min were used for all further experiments. Figure 3 shows SEM micrographs and the corresponding 2D Fast Fourier transform (2D-FTT) images of films of different ZnO nanorods (short, medium, and long growth times) aligned by slow solvent evaporation according to the described procedure. Thin films deposited by spincoating are shown as reference. Note, that due to the change of concentration during the evaporation of the solvent the final nanorod alignment depends on location along the substrate. The quality of alignment can be divided roughly in three zones. As shown in Figure 3, zone 2 at the very top shows the best alignment; in zone 1, the nanorods still exhibit some overall orientation while zone 0 at the bottom is mostly isotropic. This is also illustrated in Figure S4 in the Supporting Information. The lack of alignment in zone 0 could be due to a destabilization of the ZnO nanorod dispersion over time as evaporation takes 2−4

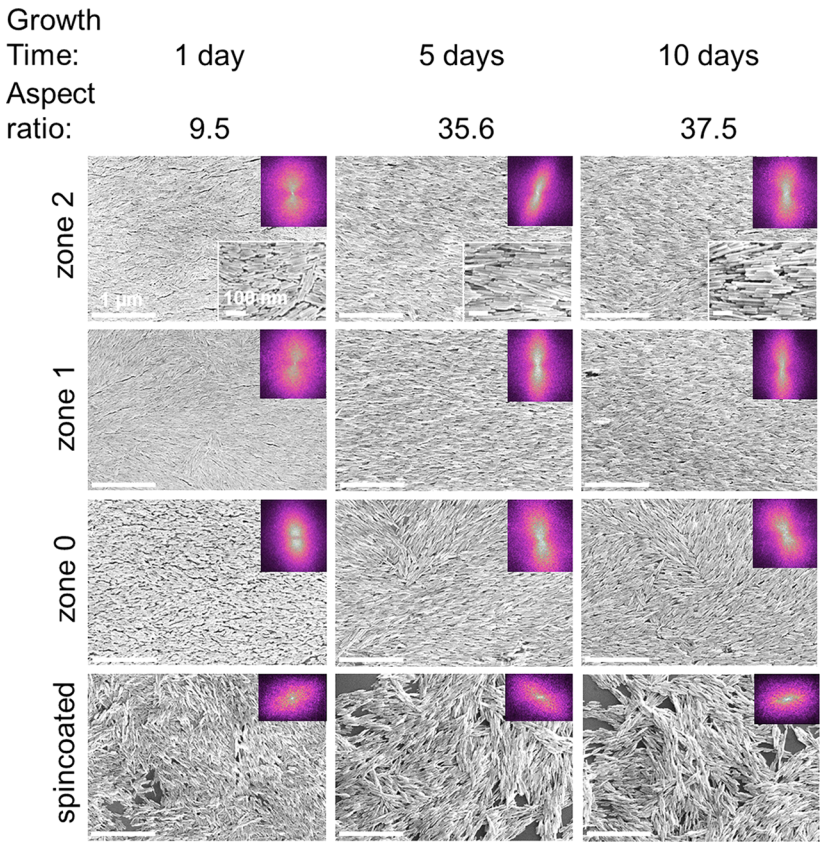

Figure 3. SEM micrographs (magnification 30 000×, scale bar 1 μm) and their 2D Fast Fourier transformation (insets) of self-assembled ZnO nanorods (aspect ratios 9.5, 35.6, and 37.5) in the upper (zone 2, higher-magnification inset: scale bar 100 nm), middle (zone 1), and lower part (zone 0) of the substrate after slow evaporation, and spin-coated ZnO nanorods as reference.

weeks to complete. Thus, nanorods may start to aggregate and lose their capability to align at the liquid−solid−air interface.

In general, ZnO nanorods with higher aspect ratios form more anisotropic layers oriented over micrometer length scales as seen for zone 2 in Figure 3 (SEM) and Figure S5 in the Supporting Information (AFM). For short nanorods the alignment is limited to small domains of hundreds of nanometers, whose orientations vary, although there is still a preference for parallel alignment with respect to the evaporation line. Despite the low aspect ratio of all of these nanorods, the increasing level of alignment with aspect ratio follows the predictions of Onsager's theory. Spincoated films of ZnO nanorods with different lengths are isotropic and show a large degree of disorder with generally poor packing density. In particular longer nanorods leave large gaps while showing some short-range alignment with adjacent nanorods. Cross sections of spincoated nanorod films (see Figure S6 in the Supporting Information) reveal large roughness and frequent out-of-plane orientation of the rods with respect to the substrate. Sun et al. showed that the order in spincoated films can be improved by further optimizing the dispersion concentration;[24] however, this was not attempted here. In contrast to the spincoated films, cross sections of nanorod films deposited by slow evaporation (Figure 4) show a large degree of in-plane alignment throughout the entire layer from top to bottom.

In summary, we achieved various degrees of order over large areas for short and long ZnO nanorods by using a slow solvent evaporation method and dispersions with relatively low concentrations. The degree of alignment is largest in a several millimeter wide zone at the top of all samples, whereas the lower parts are almost isotropic. Notably the in-plane order for layers deposited by slow evaporation is much higher than for spincoated films. Furthermore, the use of longer nanorods leads to better long-range order. The controlled alignment over macroscopic areas allows for the comprehensive characterization of electron transport in ZnO nanorod thin films with respect to orientation and length.

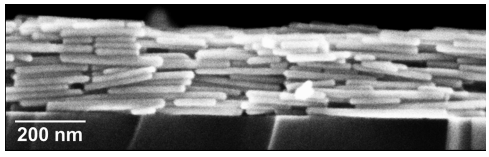

Figure 4. Cross-sectional view of aligned ZnO nanorods (aspect ratio: 35.6) from zone 2.

Charge Transport in Aligned ZnO Nanorod FETs. To study the charge transport in aligned films of ZnO nanorods, we employed electrolyte-gating with the ionic liquid [EMIM]-[TFSI], as schematically shown in Figure 1b. This allowed us to measure samples with large surface roughness, which would be difficult to test otherwise as we will show later. Figure 5a shows representative transfer characteristics of electrolyte-gated FETs based on ZnO nanorods with an average aspect ratio of 37.5 and different degrees of alignment with respect to the charge transport direction from isotropic (spincoated) to highly parallel (zone 2) and perpendicular (zone 2 perpendicular). The electrode arrangement on the substrates is shown in Figure S7 in the Supporting Information. Additional transfer and output characteristics for nanorods with an aspect ratio of 35.6

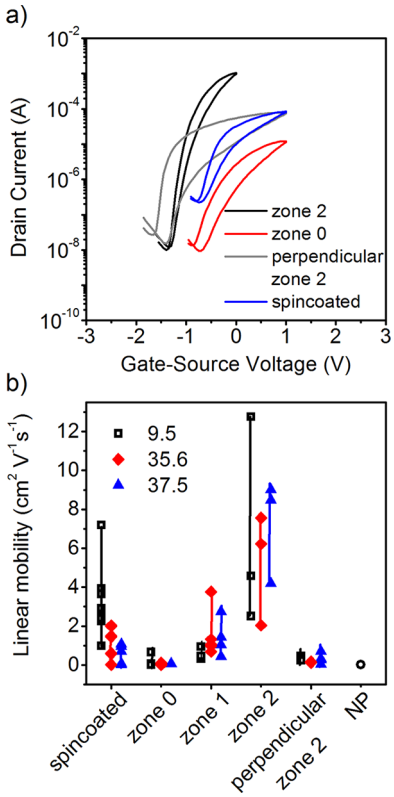

Figure 5. (a) Transfer characteristics (V_{DS} = 1.0 V) for [EMIM]-[TFSI]-gated ZnO nanorod (aspect ratio 37.5) FETs with different degrees of alignment parallel or perpendicular to the charge transport direction. (b) Linear field-effect mobilities for various nanorod lengths and degrees of alignment and 5 nm ZnO nanoparticles as reference.

are provided in the Supporting Information (Figures S8–S12). All IL-gated ZnO nanorod FETs are operating at low gate voltages with turn on-voltages (V_{ON}) between −1.4 V and −0.6 V, and threshold voltages (V_{Th}) between −0.6 and 0.1 V. The negative values for V_{Th} confirm the expected n-doping of ZnO.[37] Note that the increase of current at gate voltages more negative than V_{ON} is due to gate leakage caused by typical sweep rate-dependent charging effects in electrolyte-gated FETs. For all IL-gated ZnO-FETs the drain current (I_D) vs source-drain voltage (V_{DS}) plots show a linear current increase at small source-drain voltages (<0.2 V) indicating good ohmic contact between the ZnO and the aluminum electrodes. The drain current saturates at V_{DS} >1 V.

Distinct differences in carrier mobility, threshold voltages and hysteresis are already obvious from the current–voltage plots in Figure 5a. To estimate the general effect of length and orientation of the nanorods on electron transport, we measured up to eight devices per aspect ratio and degree of alignment (all W/L = 50) and determined average parameters. Mobilities in the linear regime were calculated according to

$$\mu_{lin} = \frac{\partial I_D}{\partial V_G}\frac{L}{WC_iV_{DS}} \quad (1)$$

and saturation mobilities using

$$\mu_{sat} = \frac{\partial I_D}{\partial V_G}\frac{L}{WC_i}\frac{1}{V_G - V_{Th}} \quad (2)$$

with W, channel width, L, channel length; C_i, specific capacitance; V_G, source-gate voltage; V_{Th}, threshold voltage; V_{DS}, source-drain voltage. The results for various ZnO nanorods and nanoparticles (diameter 5 nm) are summarized in Figure 5b for the extracted linear mobilities and in Figure S13 in the Supporting for saturation field-effect mobilities.

Table 2. Turn-on Voltage (V_{ON}), Threshold Voltage (V_{Th}), on/off Ratio, and Linear (μ_{lin}) and Saturation Mobility (μ_{sat}) for FETs with Different Degrees of Alignment of ZnO Nanorods Gated with Ionic Liquid [EMIM][TFSI] and for ZnO Nanoparticles (ZnO-NP, average diameter 5 nm) Gated via [EMIM][TFSI] or 300 nm SiO_2

	V_{ON} (V)	standard deviation	V_{Th} (V)	standard deviation	on/off current ratio	μ_{lin} ($cm^2V^{-1}s^{-1}$)	standard deviation	μ_{sat} ($cm^2\ V^{-1}\ s^{-1}$)	standard deviation
nanorods 1 day growth									
spin-coated	−1.8	0.3	−1.6	0.2	2×10^3	2.1	1.9	1.1	1.2
zone 0	−0.5	0.4	−0.2	0.5	8×10^2	0.2	0.3	0.1	0.2
zone1	−0.9	0.2	−0.2	0.7	3×10^3	0.6	0.3	0.5	0.1
zone 2	−1.2	0.1	−0.8	0.1	9×10^3	6.6	5.4	3.4	2.3
perpendicular zone 2	−2.0	0.1	−1.6	0.1	5×10^2	0.4	0.1	0.8	0.3
nanorods 5 days growth									
spin-coated	−1.4	0.1	−0.9	0.2	2×10^3	1.2	0.8	0.6	0.3
zone 0	−0.5	0.2	−0.1	0.2	6×10^2	0.1	0.1	0.1	0.1
zone 1	−1.1	0.3	−0.5	0.2	1×10^4	1.6	1.3	1.3	1.3
zone 2	−1.6	0.4	−1.0	0.5	4×10^4	5.5	2.4	4.3	0.9
perpendicular zone 2	−1.4	0.1	−0.3	0.1	2×10^3	0.2	0.1	0.1	0.06
nanorods 10 days growth									
spin-coated	−0.6	0.2	−0.2	0.1	4×10^2	0.5	0.5	0.2	0.2
zone 0	−0.6	0.2	0.1	0.1	6×10^2	0.1	0.02	0.1	0.01
zone 1	−1.3	0.5	−0.6	0.4	2×10^4	1.4	0.1	1.5	1.3
zone 2	−1.6	0.4	−1.0	0.3	4×0^4	7.2	2.6	5.5	2.5
perpendicular zone 2	−1.4	0.1	−0.6	0.3	5×10^3	0.4	0.3	0.1	0.1
nanoparticles (5 nm)									
[EMIM][TFSI]	−0.1	0.1	0.3	0.2	1×10^3	0.023	0.007	0.011	0.004
SiO_2	30	10	37	8	1×10^3	0.0028	0.0002	0.0033	0.0004

dx.doi.org/10.1021/am3026739 | ACS Appl. Mater. Interfaces 2013, 5, 1656–1662

Table 2 contains the average values of mobility, turn on-voltage, threshold voltage, and on/off ratio for all devices.

For any given length of nanorods, a higher degree of alignment along the transport direction, that is, from zone 0 to zone 2, results in higher mobilities. For example, for the longest nanorods the calculated average linear mobility increases from 0.1 $cm^2 V^{-1} s^{-1}$ in zone 0 to 7.2 $cm^2 V^{-1} s^{-1}$ in zone 2. For the perpendicular orientation in zone 2 the mobility drops dramatically to 0.4 $cm^2 V^{-1} s^{-1}$, which is similar to the mobility in spincoated films (0.5 $cm^2 V^{-1} s^{-1}$). ZnO nanoparticle-based FETs show by far the lowest mobility with an average 0.023 $cm^2 V^{-1} s^{-1}$.

Interestingly, the degree of orientation has a much larger effect on mobility than the length of the nanorods. Within the same alignment zone the mobilities for short and long nanorods vary slightly but remain within the uncertainty range for these values. The spin-coated nanorod films are the only exception. In this case the shorter nanorods actually show significantly larger average mobilities (2.1 $cm^2 V^{-1} s^{-1}$) than the ZnO nanorods with larger aspect ratios (0.5 $cm^2 V^{-1} s^{-1}$). This is most likely due to the higher packing density of shorter nanorods during spincoating, which is not attainable for spin-coated high-aspect-ratio nanorods, as also seen in the SEM images in Figure 3.

We can explain the dependence of mobility on alignment of the nanorods with the reduced number of hopping events necessary for the electrons to reach the drain electrode. The mobility within a single nanorod is quite high (up to 40 $cm^2 V^{-1} s^{-1}$)[20] and thus the apparent field-effect mobilities in ZnO nanorod layers must be limited by the number of interfaces and associated traps that need to be overcome. Clearly the parallel orientation of rods leads to fewer hopping events than perpendicular orientation. Less obvious is the lack of scaling with the length of the nanorods. Close examination of the SEM images in Figure 3 reveals that although the longer nanorods have a higher degree of alignment they are not so closely packed that every nanorod is in contact with the next rod in a straight line. A lot of charge transport has to proceed via hopping across the broad side of adjacent nanorods. The packing density, which limits this type of charge transport, is in fact slightly higher for shorter nanorods. The connectivity between the nanorods could be further improved by spincoating zinc precursor solution onto the layer followed by sintering in air, however this would require high temperatures (>200 °C).[24]

The on- and threshold voltages vary a lot from device to device. Broadly they become more negative with degree of alignment but change little with nanorod length. Current hysteresis is significantly larger for transport perpendicular to the alignment direction compared to parallel orientation for all nanorod lengths. The shift to more negative threshold voltages for higher degrees of alignment suggests that the transport threshold is determined by both the concentration of n-dopants (shift to negative voltages) in the bulk of the ZnO[37] and the number of electron traps, which have to be filled before transport can take place (shift to positive voltages). The latter are likely to be associated with surface states.[38] For well aligned nanorod films the influence of surface states should be reduced compared to poorly aligned or nanoparticle-based films because fewer hopping events from nanorod to nanorod take place. Thus n-doping of the bulk ZnO should shift the overall threshold to more negative values. The large hysteresis for devices with perpendicular nanorod orientation indicates a larger influence of shallow traps at the nanorod surfaces.

Trying to gate the aligned ZnO nanorod films in a bottom-gate configuration with SiO_2 as the dielectric instead of using electrolyte-gating results in very high drain currents (~100 μA), which cannot be modulated by the gate voltage (see Figure S14 in the Supporting Information), that is, the channel is always on. This may be due to the thickness of the nanorod layer and the use of top-contact aluminum electrodes. The influence of the gate field extends only few nm away from the dielectric interface and the ZnO nanorods are n-doped, which results in a normally on state. Thus charge transport will predominantly take place close to the top of the surface where it cannot be modulated by the gate. Also the effect of gating on nanowires depends strongly on the geometry of the gate and the gate dielectric. While the gating effect of a planar gate electrode and dielectric on nanowires is strongly limited,[20,39] the electric double layer of the ionic liquid creates an all-around gating effect and can thus efficiently tune the charge carrier density in the ZnO nanorod layers. This advantage is not limited to FETs with liquid electrolytes but should work equally well for nanorod devices with printable iongel dielectrics, which have similar properties.[32,40]

It is further helpful to compare the observed mobilities of aligned ZnO nanorods (up to 7.2 $cm^2 V^{-1} s^{-1}$) to other electrolyte-gated ZnO-based FETs. Polycrystalline, spray-coated ZnO films, which require processing temperatures of 390 °C, exhibit linear mobilities of about 3.6 $cm^2 V^{-1} s^{-1}$ measured under the same conditions in nitrogen atmosphere with the same ionic liquid.[35] These values are comparable to other solution processed, electrolyte-gated ZnO thin film transistors as for example shown by Lee et al.[40] The crystalline domain size for spray-coated ZnO is much smaller (about 19 nm) than the length of the ZnO nanorods, which may explain the lower mobility despite the formation of a continuous layer. Spincoated thin films of 5 nm ZnO nanoparticles merely reach linear field-effect mobilities of 0.023 $cm^2 V^{-1} s^{-1}$ when electrolyte-gated and only 2.8×10^{-3} $cm^2 V^{-1} s^{-1}$ when gated via SiO_2 despite their smooth film morphology. Clearly, the large number of hopping barriers and surface defects is detrimental to charge transport in both cases. The higher mobility for electrolyte-gated nanoparticle FETs compared to back-gated devices may be explained with the larger charge carrier density and thus filling of shallow traps that can be achieved with electrolyte-gating (5×10^{13} charges/cm^2 at 1 V) compared to thick SiO_2 dielectrics (9×10^{12} charges/cm^2 at 100 V). On the whole, well-aligned ZnO nanorods are outperforming other forms of solution-processed and electrolyte-gated ZnO. Even randomly oriented nanorod layers show much higher mobilities than nanoparticle films.

CONCLUSIONS

In summary, we successfully prepared ZnO nanorod thin films with varying degrees of alignment from isotropic to highly oriented for three different nanorod aspect ratios by exploiting the self-assembly properties of the colloidal dispersions at the liquid–solid-air interface during slow evaporation of the solvent. We showed that electrolyte-gating with ionic liquids is an efficient way to modulate the charge carrier density and thus the drain current in ZnO nanorod field-effect transistors, while traditional bottom-gate structures fail in this regard. Electron mobilities depend highly on the degree of alignment but less on the length of the nanorods. The very low processing

temperatures and high linear mobilities (up to 9 $cm^2 V^{-1} s^{-1}$) for well-aligned ZnO nanorods compare very favorably with other solution-processed ZnO FETs. However, for large scale production the deposition rate is too slow and alternative and faster ways of achieving the same degree of alignment, e.g., by applying shear, should be explored.

■ ASSOCIATED CONTENT

Supporting Information

SEM and TEM images of nanorods, optical micrographs of ZnO nanorod thin films depending on concentration and evaporation rate, their division into zones with corresponding SEM and AFM images, SEM image of thin film cross-sections, representative transfer and output characteristics for FETs with different degrees of nanorod alignment, transfer and output characteristics of FETs with 5 nm ZnO nanoparticles, absorption spectra of a dispersion of 5 nm ZnO nanoparticles are presented in the Supporting Information. This material is available free of charge via the Internet at http://pubs.acs.org.

■ AUTHOR INFORMATION

Corresponding Author

*E-mail: jana.zaumseil@ww.uni-erlangen.de.

Notes

The authors declare no competing financial interest.

■ ACKNOWLEDGMENTS

The authors acknowledge funding by the Deutsche Forschungsgemeinschaft (DFG) via the Research Training Group 'Disperse Systems for Electronic Applications' (GRK 1161) and the Cluster of Excellence 'Engineering of Advanced Materials' (EXC 315), and are grateful for support by Evonik Industries AG.

■ REFERENCES

(1) Anthony, J. E. *Chem. Rev.* **2006**, *106*, 5028−5048.
(2) Rouhi, N.; Jain, D.; Burke, P. J. *ACS Nano* **2011**, *5*, 8471−8487.
(3) Fortunato, E.; Barquinha, P.; Martins, R. *Adv. Mater.* **2012**, *24*, 2945−2986.
(4) Talapin, D. V.; Lee, J.-S.; Kovalenko, M. V.; Shevchenko, E. V. *Chem. Rev.* **2010**, *110*, 389−458.
(5) Lee, J.-S.; Kovalenko, M. V.; Huang, J.; Chung, D. S.; Talapin, D. V. *Nat. Nanotechnol.* **2011**, *6*, 348−352.
(6) Talapin, D. V.; Black, C. T.; Kagan, C. R.; Shevchenko, E. V.; Afzali, A.; Murray, C. B. *J. Phys. Chem. C* **2007**, *111*, 13244−13249.
(7) Kim, D. K.; Vemulkar, T. R.; Oh, S. J.; Koh, W.-K.; Murray, C. B.; Kagan, C. R. *ACS Nano* **2011**, *5*, 3230−3236.
(8) Kim, D. K.; Lai, Y.; Vemulkar, T. R.; Kagan, C. R. *ACS Nano* **2011**, *5*, 10074−10083.
(9) Faber, H.; Burkhardt, M.; Jedaa, A.; Kälblein, D.; Klauk, H.; Halik, M. *Adv. Mater.* **2009**, *21*, 3099−3104.
(10) Sun, B.; Sirringhaus, H. *Nano Lett.* **2005**, *5*, 2408−2413.
(11) Kovalenko, M. V.; Scheele, M.; Talapin, D. V. *Science* **2009**, *324*, 1417−1420.
(12) Chung, D. S.; Lee, J. S.; Huang, J.; Nag, A.; Ithurria, S.; Talapin, D. V. *Nano Lett* **2012**, *12*, 1813−1820.
(13) Adamopoulos, G.; Bashir, A.; Thomas, S.; Gillin, W. P.; Georgakopoulos, S.; Shkunov, M.; Baklar, M. A.; Stingelin, N.; Maher, R. C.; Cohen, L. F.; Bradley, D. D. C.; Anthopoulos, T. D. *Adv. Mater.* **2010**, 4764−4769.
(14) Adamopoulos, G.; Bashir, A.; Gillin, W. P.; Georgakopoulos, S.; Shkunov, M.; Baklar, M. A.; Stingelin, N.; Bradley, D. D. C.; Anthopoulos, T. D. *Adv. Funct. Mater.* **2011**, *21*, 525−531.
(15) Adamopoulos, G.; Thomas, S.; Wöbkenberg, P. H.; Bradley, D. D. C.; McLachlan, M. A.; Anthopoulos, T. D. *Adv. Mater.* **2011**, *23*, 1894−1898.
(16) Li, C.-S.; Li, Y.-N.; Wu, Y.-L.; Ong, B.-S.; Loutfy, R.-O. *J. Mater. Chem.* **2009**, *19*, 1626−1634.
(17) Carcia, P. F.; McLean, R. S.; Reilly, M. H.; Nunes, G. *Appl. Phys. Lett.* **2003**, *82*, 1117−1119.
(18) Miyamoto, K.; Sano, M.; Kato, H.; Yao, T. *J. Cryst. Growth* **2004**, *265*, 34−40.
(19) Tsukazaki, A.; Yuji, H.; Akasaka, S.; Tamura, K.; Nakahara, K.; Tanabe, T.; Takasu, H.; Ohtomo, A.; Kawasaki, M. *Appl. Phys. Express* **2008**, *1*, 055004.
(20) Kälblein, D.; Weitz, R. T.; Böttcher, H. J.; Ante, F.; Zschieschang, U.; Kern, K.; Klauk, H. *Nano Lett.* **2011**, *11*, 5309−5315.
(21) Liu, J.-W.; Liang, H.-W.; Yu, S.-H. *Chem. Rev.* **2012**, *112*, 4770−4799.
(22) Engel, M.; Small, J. P.; Steiner, M.; Freitag, M.; Green, A. A.; Hersam, M. C.; Avouris, P. *ACS Nano* **2008**, *2*, 2445−2452.
(23) Onsager, L. *Ann. N.Y. Acad. Sci.* **1949**, *51*, 627−659.
(24) Sun, B.; Peterson, R. L.; Sirringhaus, H.; Mori, K. *J. Phys. Chem. C* **2007**, *111*, 18831−18835.
(25) Ye, X.; Jin, L.; Caglayan, H.; Chen, J.; Xing, G.; Zheng, C.; Doan-Nguyen, V.; Kang, Y.; Engheta, N.; Kagan, C. R.; Murray, C. B. *ACS Nano* **2012**, *6*, 2804−2817.
(26) Ghezelbash, A.; Koo, B.; Korgel, B. A. *Nano Lett.* **2006**, *6*, 1832−1836.
(27) Ghosh, M.; Fan, F.; Stebe, K. J. *Langmuir* **2007**, *23*, 2180−2183.
(28) Watanabe, S.; Inukai, K.; Mizuta, S.; Miyahara, M. T. *Langmuir* **2009**, *25*, 7287−7295.
(29) Cao, H.; Lan, D.; Wang, Y.; Volinsky, A.; Duan, L.; Jiang, H. *Phys. Rev. E* **2010**, *82*, 031602.
(30) Cho, J. H.; Lee, J.; Xia, Y.; Kim, B.; He, Y.; Renn, M. J.; Lodge, T. P.; Frisbie, C. D. *Nat. Mater.* **2008**, *7*, 900−906.
(31) Cho, J. H.; Lee, J.; He, Y.; Kim, B. S.; Lodge, T. P.; Frisbie, C. D. *Adv. Mater.* **2008**, *20*, 686−690.
(32) Lee, J.; Kaake, L. G.; Cho, J. H.; Zhu, X. Y.; Lodge, T. P.; Frisbie, C. D. *J. Phys. Chem. C* **2009**, *113*, 8972−8981.
(33) Kang, M. S.; Lee, J.; Norris, D. J.; Frisbie, C. D. *Nano Lett.* **2009**, *9*, 3848−3852.
(34) Segets, D.; Gradl, J.; Taylor, R. K.; Vassilev, V.; Peukert, W. *ACS Nano* **2009**, *3*, 1703−1710.
(35) Thiemann, S.; Sachnov, S.; Porscha, S.; Wasserscheid, P.; Zaumseil, J. *J. Phys. Chem. C* **2012**, *116*, 13536−13544.
(36) Voigt, M.; Klaumünzer, M.; Thiem, H.; Peukert, W. *J. Phys. Chem. C* **2010**, *114*, 6243−6249.
(37) McCluskey, M. D.; Jokela, S. J. *J. Appl. Phys.* **2009**, *106*, 071101.
(38) Faber, H.; Hirschmann, J.; Klaumünzer, M.; Braunschweig, B.; Peukert, W.; Halik, M. *ACS Appl. Mater. Interfaces* **2012**, *4*, 1693−1696.
(39) Khanal, D. R.; Wu, J. *Nano Lett.* **2007**, *7*, 2778−2783.
(40) Lee, K. H.; Kang, M. S.; Zhang, S.; Gu, Y.; Lodge, T. P.; Frisbie, C. D. *Adv. Mater.* **2012**, *24*, 4457−4462.